Modelling of High-performance Envelope and Façade Integrated Photovoltaic/Solar Thermal Systems for High-Latitude Applications

Yichao Chen, Andreas Athienitis, and Paul Fazio
Center for Zero Energy Building Studies, Department of Building, Civil, and Environmental Engineering, Concordia University, Montreal, Canada

Abstract

Northern housing entails both climatic and socio-economic challenges. Severe weather, high energy cost and fuel dependency on external supply call for a high-performance envelope system that can generate energy from renewable sources while functioning effectively as a passive building enclosure.

This paper presents the methods and algorithms of modelling passive solar potential and innovative façade integrated solar technologies for high-latitude applications. Custom thermal network models for different collectors are developed in MATLAB for steady state and transient analyses. Simulation results are validated through experiments under a solar simulator with a prototype combining components such as unglazed transpired collector (UTC), transpired glazing (TG), and photovoltaic/thermal (PV/T) collectors on structural insulated panel (SIP) wall. The research work aims to evaluate the potential of energy conservation and renewable generation by the proposed solar facades designed for Northern locations.

1 Introduction

Canada's North (Yukon, Northwest Territories, Nunavut) accounts for 0.3 percent of Canadian population and over one-third of the total land area. With a population of just over 100,000 dispersed across 3.5 million square kilometres of latitude 55°N and beyond, Northern housing is confronted by challenges ranging from severe *climatic* loads including low temperature, seasonal sun, harsh weather and short building season, to unique *socio-economic* issues such as housing shortage, fuel/material dependency on external supply, and extreme transportation/energy cost. Electricity price per kilowatt-hour (kWh) in some Northern communities is over 10 times higher than the Canadian average and per capita energy cost in the North is almost double the national average (National Energy Board 2011).

In response to the high heating loads and costly energy, Northern housing design is motivated to move towards greater building efficiency and the harnessing of renewable energy. In 2009, the province of Yukon announced the SuperGreen housing standard, following the most stringent building energy compliance nation-wide with prescriptive requirements of RSI-4.93 walls and RSI-10.56 ceilings, as well as triple glazed windows not exceeding 15% of gross wall area (Yukon Housing Corporation 2009).

Building envelope can also serve beyond its traditional role as a passive enclosure. Emerging development of building-integrated photovoltaic and solar thermal technologies (Athienitis et al. 2011) allows designers to integrate an active energy-capturing skin as part of the envelope system. In fact, the high energy cost and dependency on imported fuel in Northern communities offers a more competitive payback time for well-researched renewable technologies such as the photovoltaic (PV) and solar thermal. Compared to southern locations, the marginal price increase per kWh produced by solar panels is quickly offset by the reduction of expensive fossil fuel and associated transportation cost for remote locations.

2 The Northern Energy Pattern

Though rich in natural resources such as crude oil and natural gas, the Canadian North relies almost completely on imported fuel from Southern locations where raw fossil fuel is refined and processed. Energy from renewable sources constitutes a negligible amount (< 0.02% for solar and <0.12% for wind) of the total electricity use (National Energy Board 2011). For instance, Nunavut uses 100% diesel-generated electricity with small decentralized grids. The unique energy pattern and fossil fuel dependency in Northern communities entails high potential for building-integrated solar technologies.

Contrary to common perception, the Canadian North has abundant potential for solar energy. For south-facing photovoltaic panels with latitude tilt, the yearly PV potential for Iqaluit (Latitude 63.8°N, 1059 kWh/kW) and Fort Smith (Latitude 60°N, 1126 kWh/kW), are comparable to, or even higher than, southern locations like Montreal (Latitude 45°N, 1185 kWh/kW) and Halifax (44.7°N, 1074 kWh/kW) (Natural Resource Canada 2007).

The major challenge pertaining to solar utilization in the North is the strong seasonal pattern of daily global radiation and its misalignment with heating loads (e.g. long daylight hours in the summer and almost no sunlight in the winter when heating load is the highest). Therefore, the design objective of a building-integrated solar system in the North is to maximize efficiency and output in shoulder seasons, while imported fuel is still necessary for winter heating. Due to the low incidence angle of solar radiation at high latitudes, façade integration of solar panels (PV or thermal) yields better annual results than roof integration.

3 High Performance Building Envelope System and Passive Solar Potential for High-Latitudes

Norling et al. (2006) outlined the design of a low energy house in Sisimiut (67°N), Greenland. With careful design and installation of a well-insulated, air-tight building envelope, the 200m^2 house consumes only half the energy permitted in the building code. Based on this case study, Vladykova et al (2008) performed sensitivity analysis in Bsim to model the effects of changing insulation thickness and window types. Optimal south-facing window area to effectively capture solar gains is also discussed.

In Canada, wood-frame structures are currently the main form of residential construction in the North. However, labour shortage and limited transportation and building season are major roadblocks associated with budget and timeline for Northern housing. For the scope of this paper, a pre-fabricated high-performance envelope system, Structural Insulated Panel (SIP), is modelled using thermal network in frequency domain (admittance method) to investigate the interlinked effects of varying window-to-wall ratio (WWR), building insulation (RSI) and thermal mass using phase-change-material (PCM) floor tiles. While a dynamic simulation model would be more suited for PCM storage which behaves in a non-linear manner, the admittance method is employed only as a simple linear approximation.

The unique SIP system used in this model was developed for Nunavut social housing in 2009. It is composed of two 16 mm oriented strand board (OSB) skins sandwiching 273 mm of rigid expanded polystyrene (EPS), bonded by urethane glue that also acts as the vapor barrier. Each SIP panel is manufactured with wood I-joists, thermal breaks and gaskets at joints and serves as an all-in-one system of structure, insulation and air/weather barrier and vapor control. Extremely well insulated and air-tight, the SIP house offers a wall RSI of 7.9 m^{2}K/watt and a blower-door tested air tightness of 0.2ACH at 50Pa.

A single-family SIP house of aspect ratio 1.3 (Figure 1, left) is used in clear-day simulation using weather data of Iqaluit. Only south-facing windows are taken into consideration when calculating solar gains. Triple-glazed argon filled windows with U-value of 1.115 W/m^2/K are used. Effective beam transmittance varying with incidence angles are

calculated from extinction coefficients. Effective transmittance for diffused sunlight is approximated as the value of beam transmittance at incidence angle of 60°. Insulation level from RSI 2 to10 are plotted by varying the thickness of EPS in the SIP wall system. Roof and floor panels use a constant value of RSI-10.57 (equivalent R-60).

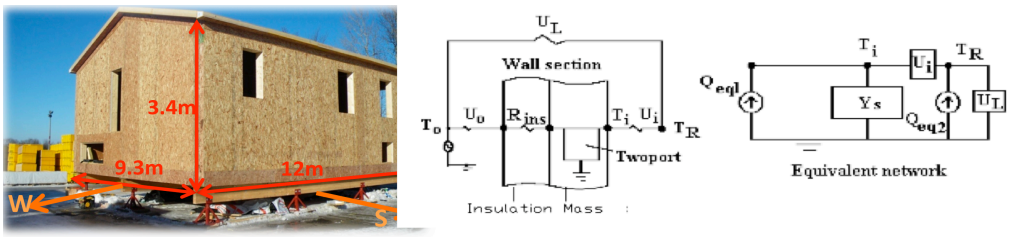

Fig. 1 Left: SIP house used in model; Right: Norton equivalent network for exterior wall

The Norton equivalent network for exterior wall is illustrated in Figure 1 (Athienitis&Santamouris 2002). Consider wall, roof, or floor panel made up of exterior insulation (SIP) and inner storage mass layer (gypsum board, carpet, or phase-change material tiles). The heat transfer from room side (1) to outside (2) can be written in matrix form:

$$\begin{bmatrix} T_1 \\ q'_1 \end{bmatrix} = \underbrace{\begin{bmatrix} D & B \\ C & D \end{bmatrix}}_{\substack{\text{mass} \\ \text{cascade} \\ \text{matrix}}} \cdot \underbrace{\begin{bmatrix} 1 & 1/h_o \\ 0 & 1 \end{bmatrix}}_{\substack{\text{insulation} \\ \text{\& air cascade} \\ \text{matrix}}} \begin{bmatrix} T_2 \\ -q'_2 \end{bmatrix} = \underbrace{\begin{bmatrix} D & D/h_o + B \\ C & C/h_o + D \end{bmatrix}}_{\text{wall cascade matrix}} \cdot \begin{bmatrix} T_2 \\ -q'_2 \end{bmatrix} \tag{1}$$

where h_o is the overall thermal conductance of the wall and air films (W/m^2K) and the mass cascade matrix describes the thermal mass (B, C, D are variables in the frequency domain expressed by complex numbers) with calculation details in Athienitis&Santamouris (2002). If $T_1(=T_{in})$ is temporarily set to zero, one can obtain transfer admittance Y_{12} that quantifies how heat flows from port 1 to 2 (inside to outside). Similarly, the self-admittance Y_{11} can be found by temporarily setting T_2 ($=T_O$) equal to zero and rearranging the matrix. Note that admittance (Y) matrix is written as:

$$\begin{bmatrix} q'_1 \\ q'_2 \end{bmatrix} = \begin{bmatrix} Y_{11} & Y_{12} \\ Y_{21} & Y_{22} \end{bmatrix} \cdot \begin{bmatrix} T_1 \\ T_2 \end{bmatrix} \tag{2}$$

Assuming a constant indoor temperature of 20°C, total heat loss from the SIP house is evaluated as the sum of heat loss from the SIP envelope (Y_{11} and Y_{12}), windows (depends on WWR), and infiltration (0.2 ACH). Figure 2 shows the overall heat loss of the SIP house at different wall RSI and WWR (defined as south-facing window area over south wall area). Zone heat loss are plotted at WWR=0.1 and 0.3 in April (clear day, 2a) and November (with no sun, 2b), as well as at WWR=0.2 for clear days in May (2c), and June (2d).

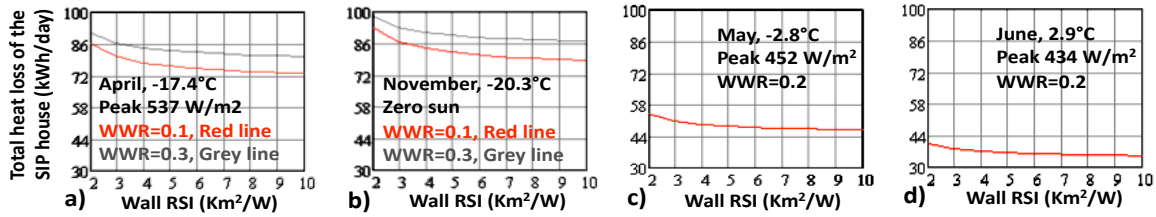

Fig. 2 Total daily heat loss of SIP house with constant 20°C indoor and auxiliary HVAC

As can be seen from the ubiquitous trend in Figure 2, increasing insulation up to RSI-4 results in steep reduction in heat loss, indicating a minimum of RSI-4 is necessary for Iqaluit to avoid excessive heat loss. From RSI4 to RSI7, significant heat loss reduction can be observed at a diminished rate and the effort is still worthwhile as it is relatively cheap to build to RSI-7. Yet, for values beyond RSI-10, the zone heat loss is characterized by the flat tail

when the benefit of reducing heating loads cannot be justified by the increased cost of insulation. Alternatively, one should consider investing in better windows or active solar components. The red and grey lines in Figure 2 (a and b) suggest that optimizing window area also contributes to the reduction of heating loads, especially for Nordic locations with long, dark winters when windows act like thermal bridges. In addition, the upper limit of WWR is confined by the possibility of overheating during mild sunny days.

For a clear day in April with transmitted peak solar irradiance of 537 W/m^2, the passive room temperature response as a function of different WWR and RSI is plotted in Figure 3, assuming that no auxiliary HVAC interferes with room temperature in this case.

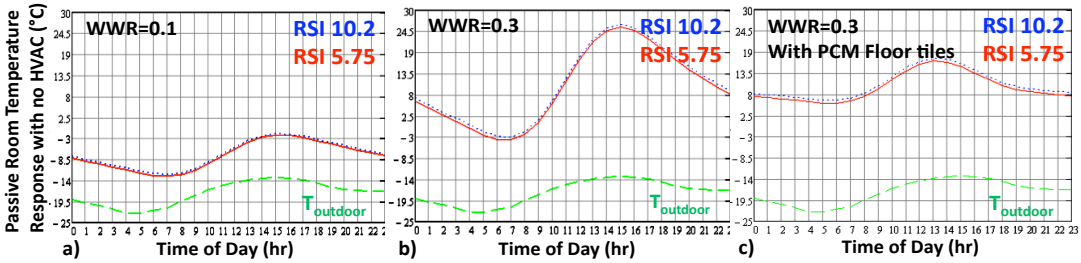

Fig. 3. Room temperature – passive response to solar gains (April), no auxiliary HVAC

The transient indoor temperature variation is a function of the amount of solar gains and zone heat losses. Room temperature peaks at 3pm. Note that both average value and peak amplitude increased with increasing WWR (Figure 3a and 3b). To evaluate the effect of thermal mass, a thin layer of DuPont EnerGain PCM tiles (storage temperature range 14 to 30 °C) is added to the floor interior. The addition of PCM is approximated linearly as an equivalent thermal capacity on the floor. As a result, room temperature is comparatively less variant with time (Figure 3c) while maintaining the same average value as Figure 3b, since thermal mass does not change the amount of transferred solar gains.

In conclusion, the passive solar house design techniques can be effectively extended to Arctic regions. The optimal wall insulation level from this analysis lies between RSI 7 to 10, the exact value of which largely depends on the marginal cost of insulation, window types and WWR. Movable blinds are necessary for cases of WWR>0.2 to avoid overheating in the summer. Night insulation for windows (insulated shutters) may also be used to reduce night time heat losses. Thermal storage beyond the gypsum boards is needed to smooth out the room temperature peak as a result of solar gains. As light-weight construction materials with little thermal mass are predominant in Northern housing due to the high transportation cost, light-weight PCM tiles or drywall offer a competitive solution as thermal storage in residential buildings. Lastly, the pre-fabricated nature of SIP system can be extended to incorporate a potential solar harnessing skin as exterior cladding on the SIP panel.

4 Building-Integrated Photovoltaic/Solar Thermal Systems for the North

4.1 Unglazed Transpired Collector

Unglazed Transpired Collector (UTC) is essentially a perforated dark cladding with pores of 0.5%-2% opening area and an air cavity/plenum behind the cladding. It is a low-cost and highly efficient solar thermal system that is well suited for façade integration to pre-heat ventilation air in residential and commercial buildings. At night, the air plenum also recaptures heat loss from the building envelope and contributes to the overall energy savings.

Compared to conventional glazed solar thermal collectors, the distributed air inlets across the cladding (absorber) help to lower the surface temperature of UTC (hence less surface radiant loss), which works particularly well in Northern cold climate. Many of such

UTC facades have already been implemented in the far North in latitudes as high as 68°N (Inuvik) to pre-heat building ventilation air. Reflected sunlight from the snow (albedo>0.8) in early spring and late fall further enhances the system performance, partially compensating for the shorter usable duration at high latitudes. In this paper, only air-based collectors are discussed to avoid encountering risks of winter freezing as in liquid-based collectors.

4.2 Improved Transpired Collectors

Commercially available UTC systems commonly use corrugated dark metal sheets perforated with distributed pores to reduce surface temperature (Figure 4b). However, since the absorber of such a UTC system is the exterior metal cladding that is inevitably heated by solar radiation, its surface temperature can still rise by over 40 °C greater than ambient temperature on a sunny day at low heat removal rate, contributing to significant surface losses.

In addition to the surface radiant loss due to cladding temperature rise, the unglazed transpired systems are particularly prone to convective wind loss, often aggravated by the corrugated profile. For Northern applications when wind is strong (> 4m/s) year round, a flat exterior surface with lower surface temperature would be preferable in cold, windy regions.

Therefore, an improved UTC system is proposed with transpired glazing (TG) as the exterior layer (Figure 4d). High-transmittance weather-resistant polycarbonate sheets are perforated to 1% porosity and are used to create an second air plenum in front of the transpired absorber. As the exterior layer (flat transpired glazing) remains cold during the sun-lit hours, the surface radiant loss and convective wind loss are both minimized for **UTC+TG** system compared to conventional UTC system.

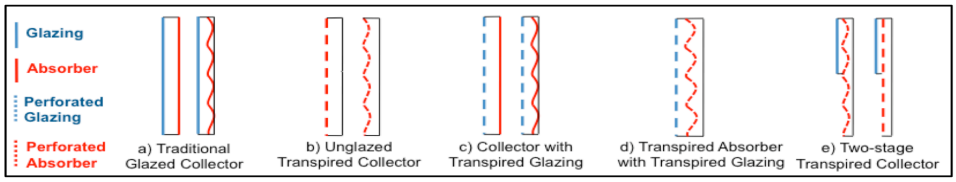

Fig. 4. Design of façade collector configurations combining UTC and transpired glazing

4.3 Photovoltaic Panel doubles as Thermal Absorber (PV/T)

Photovoltaic (PV) technology offers a reliable, on-site, complementary source of energy in summer and shoulder seasons at a competitive price rate for the North. In 1995, a 3.2kWp PV system was installed over 25m^2 of façade in Iqaluit (63.8°N) and has been delivering an average of 2016±200kWh of electricity annually (Poissant et al. 2004). Since then, PV module prices have dropped from CAD$11.09/watt in 1999 to $3.31/watt in 2009 (Ayoub et al. 2009). Using façade-integrated PV also obviates the need for exterior cladding and can be pre-fabricated with envelope panels to further reduce the installation and labour cost.

Low incidence angle, spectral shift, and low irradiance level can significantly reduce the electric efficiency of PV. TamizhMani et al. (1998) concluded a 33% efficiency reduction for façade mounted PV in Iqaluit. Yves Poissant (2009) investigated four types of flat-plate PV technologies under different climates and experimental results shown that crystalline PV (c-PV) is best suited for low light conditions with high diffused content in Northern locations.

As most crystalline photovoltaic panels yield 10% to 20% of electric efficiency, the rest of absorbed solar energy is turned into waste heat. A photovoltaic/thermal system can cogenerate valuable electricity as well as useful heat by actively drawing the heated air behind the PV module. A commercial-scale solar facade with UTC and the PV/T technology has been implemented in Montreal (45°N) in 2009 based on an outdoor prototype studied by Athienitis et al. (2011). Custom-sized dark-framed PV panels are integrated onto the dark corrugated transpired metal cladding, covering 70% of the total 288 m^2 area (Figure 5).

In addition to the electricity generation, heat is actively drawn from the back of the PV modules and the exposed UTC pores (Figure 5), contributing to heating the ventilation air while cooling the PV panels. In many regions of Northern Canada where space heating is needed almost all year round, cogeneration adds incentives to such building-integrated photovoltaic/thermal (BIPV/T) systems.

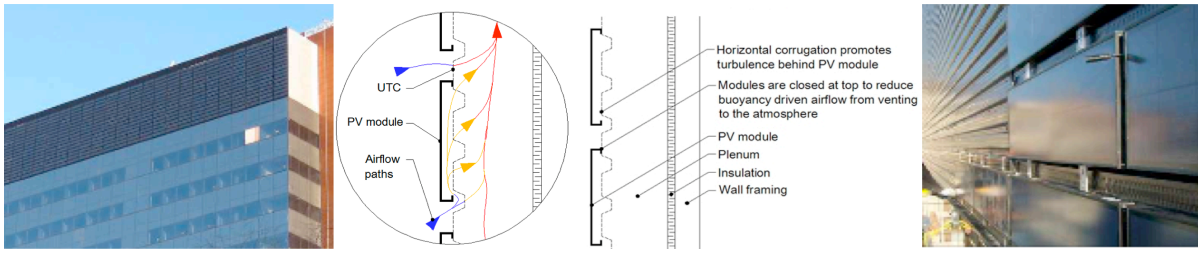

Fig. 5. A BIPV/T demonstration project using UTC and PV/T (Athienitis et al. 2011)

5 Evaluation of a BIPV/T-SIP Prototype for High Latitude Applications

5.1 Prototype Design and Testing Capacity

Façade integrated solar technologies, such as the photovoltaic and unglazed transpired collector, have been proven to perform well in the high North. In an effort to synthesize the advantages of similar solar collectors and experimentally evaluate their suitability to the Northern climate, a facade-integrated solar prototype is designed and constructed to accommodate twelve testing configurations. Each layer of the test assembly can be taken apart and reattached easily, allowing changes in configuration as experiments move forward. The components of the whole test assembly are numbered and illustrated in Figure 6 below.

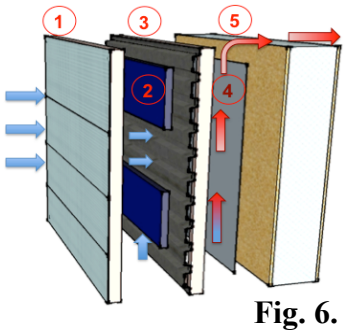

1. Transpired Glazing and/or Glazing
2. Photovoltaic Panels (60W) with dark frame and backing
3. Corrugated Transpired Absorber (can be rotated 90°)
4. Dark metal Absorber
5. Structural Insulated Panel (SIP) Wall (Substrate)

Fig. 6. BIPV/T-SIP Prototype Experimental Assembly

The prototype is designed to be square (1.5m x 1.5m) and the corrugated absorber can be rotated 90° to create scenarios of flow-against-corrugation and flow-along-corrugation. The transpired glazing is designed to be level with the photovoltaic panels. The pitch (14mm) and pore diameter (1.6mm) of the transpired glazing is carefully selected to maximize system efficiency within practical limits, based on the work of Leon&Kumar (2006) modelling the effects of pitch, pore size and porosity on transpired collector performance.

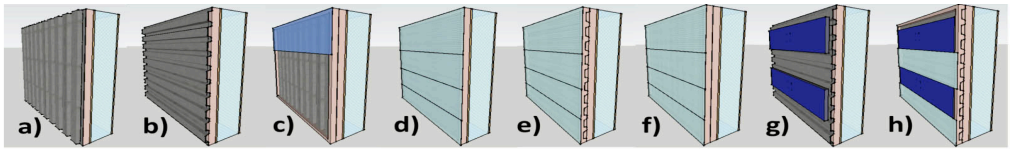

Fig. 7. Test Configurations: 7a/7b. UTC corrugation along flow(a) and against flow(b); 7c. Two-stage UTC with top glazing; 7d. Collector with Transpired Glazing (only); 7e/7f. Transpired Absorber (UTC) covered with Transpired Glazing (TG), absorber corrugation against flow(e) and along flow(f); 7g. UTC with PV/T (PV coverage 50%, similar to Figure 5); 7h. UTC with PV/T and transpired glazing (UTC+PV/T+TG)

Some of the test configurations using the same basic experimental prototype are illustrated in Figure 7 above. Among the total of twelve configurations tested, the experimental results are used to validate and calibrate simulation outputs of several important collector types (7a, 7f, 7g, and 7h), discussed in Section 6.

5.2 Experimental Investigation

The test facility for prototype testing is a two-part laboratory consisting of a Solar Simulator and a two-storey Environmental Chamber. Eight special metal halide (MHG) lamps are used to produce dense multiline spectrum of rare earth metals very comparable to continuous solar spectrum. Different collectors are evaluated at steady state conditions as shown in Table 1.

Table 1: Steady-State Testing Conditions (Solar Simulator Testing)

Solar Irradiance (±5% uniformity)	Surface Wind Speed	Mass Flow Rate
High Gain (HG): 1148 watt/m^2	High Wind (HW): 3.5m/s	150, 125, 100, 75, 50 kg/hr/m^2
Low Gain (LG): 838 watt/m^2	Low Wind (LW): 1m/s	

Each configuration undergoes four sets of tests (HG-HW, HG-LW, LG-HW, LG-LW), with five mass flow rates in each test set. Figure 8 shows several important collector configurations during solar simulator testing, among which Figure 8a (corresponds to Figure 7a), 8c (7f), 8d (7g), and 8e (7h) are modelled in Section 6.

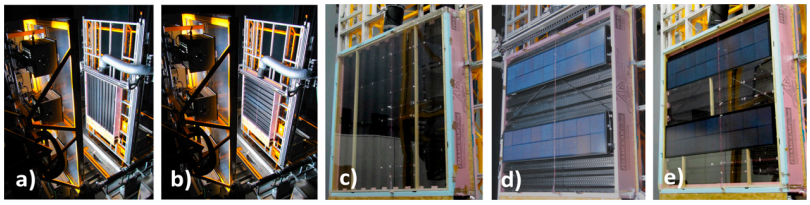

Fig. 8a/8b. UTC corrugation along flow (a) and against flow (b) under testing in the Solar Simulator Facility; 8c. UTC+TG (see Figure 7f.); 8d. UTC+PV/T (see Figure 8g.); 8e. UTC+PV/T+TG (see Figure 7h.);

In the future, the prototype will also be evaluated under ambient temperature as low as -40°C in the Environmental Chamber facility to determine the collector suitability for extreme Northern climate (e.g. icing at pores, surface loss at low temperature, etc).

6 Thermal Modelling of the BIPV/T-SIP Collectors

6.1 Thermal Models of Two Transpired Collectors

Due to the highly innovative nature of some collectors mentioned in Section 5, custom thermal network models are needed to evaluate their performance. MATLAB/Simulink is chosen as the main modelling platform for its computational power and graphic interface.

Heat Transfer in conventional UTC (Figure 6b, 7a, and 8a) has been modelled by Dymond& Kutscher (1997) assuming uniform suction rate at the surface. The energy balance of the UTC system (Figure 9, left) can be described by the following equation:

$$Q_s = Q_{RO} + Q_{wind} + Q_u + Q_b = (h_R + h_{wind}) \cdot (T_{surf} - T_{amb}) + MFR \cdot c_p \cdot (T_{plm} - T_{amb}) + h_b (T_b - T_{room}) \quad (3)$$

where Q_s is the absorbed solar radiation (W/m^2), Q_{RO} is the radiant loss to the outside (W/m^2), Q_{wind} is the convective heat loss due to wind (W/m^2), Q_u is the useful heat transferred into the building (W/m^2), and Q_b is the heat loss at the back of the collector (W/m^2); h_R is the radiant heat transfer coefficient to outside (W/m^2/K), h_{wind} is the convective heat transfer

coefficient due to wind (W/m^2/K), *MFR* is the mass flow rate (kg/s/m^2), c_p is the specific heat capacity of air (J/kg/K), h_b is the combined heat transfer coefficient of wall insulation and interior air film (W/m^2/K), all temperatures (K) are illustrated in Figure 9.

Similarly, for an improved transpired collector with transpired glazing cover (UTC+TG, Figure 6d, 7f, or 8c), system energy balance in Figure 9 (right) can be written as:

$$Q_{s1} + Q_{s2} = Q_{RO} + Q_{wind} + Q_u + Q_b \tag{4}$$

where Q_{s1} *and* Q_{s2} are the absorbed solar radiation by collector surface (transpired glazing) and by the transpired absorber (W/m^2), respectively. Q_{S1} is relatively small compared to Q_{S2}, as the transpired glazing transmits more than 90% of solar radiation to the absorber.

For prototype testing in the laboratory, a thin insulation of only RSI-1.32 is provided at the back of collector. Therefore, Q_b cannot be ignored in steady state simulations. For SIP houses of RSI-7.3 walls, Q_b is significantly reduced and transient simulation (Section 7.2) is adjusted accordingly. Note that heat recaptures at night by the air plenum are not considered.

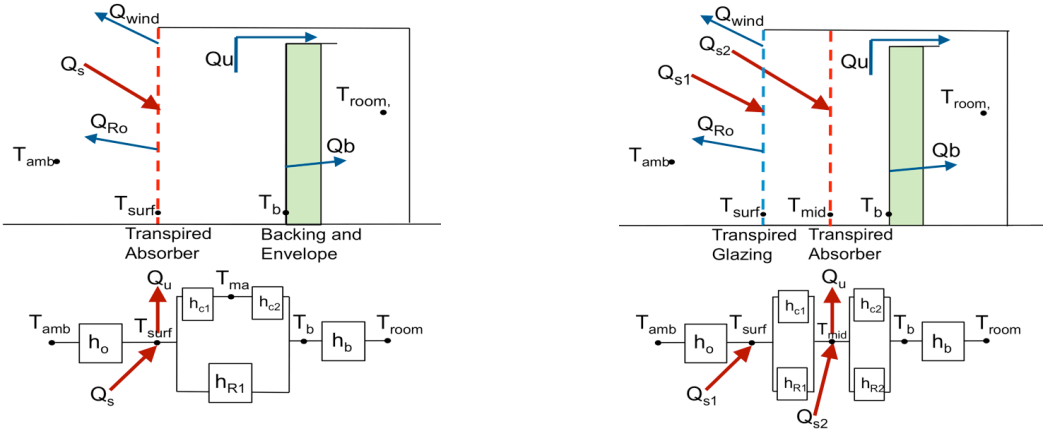

Fig. 9. Energy Balance and Thermal Network models of two transpired collectors. Left: UTC (Figure 6a, 7a, 8a); Right: UTC+TG (Figure 6d, 7f, 8c). Plenum exaggerated.

Surface Temperature can be evaluated via the energy balance for UTC (Figure 9, left) and for UTC+TG (Figure 9, right):

$$T_{surf\_UTC} = \frac{Q_s + (h_R + h_{wind}) \cdot T_{amb} + h_{R1} \cdot T_b + h_{C1} \cdot T_{ma} + MFR \cdot c_p \cdot \varepsilon_{hx} \cdot T_{amb}}{h_R + h_{wind} + h_{R1} + h_{C1} + MFR \cdot c_p \cdot \varepsilon_{hx}} \tag{5}$$

$$T_{surf\_UTC+TG} = \frac{Q_{S1} + (h_R + h_{wind}) \cdot T_{amb} + (h_{R1} + h_{C1}) \cdot T_{mid}}{h_R + h_{wind} + h_{R1} + h_{C1}} \tag{6}$$

where ε_{hx} is the effectiveness of UTC, T_{ma} is a fictitious temperature assumed to describe air at mid-plenum (K) for UTC, T_b is the temperature (K) at the back plate of collectors. T_{ma} and T_b can both be calculated via the thermal network model illustrated in Figure 9 (left). For the normal UTC, h_{C1} and h_{C2} are the convective heat transfer coefficients of the two interior surfaces in the air plenum (W/m^2/K). For *UTC+TG*, h_{C1} and h_{C2} are the combined convective heat transfer coefficients of the two interior plenums (W/m^2/K) as seen in Figure 9 (right).

All the convective heat transfer coefficients are calculated according to the experimental data obtained for normal and improved UTC. In particular, the convective heat transfer coefficient due to wind (h_{wind}) takes the empirical form of equation 7 (Palyvos 2008):

$$h_{wind} = a \cdot V_{wind}^b \cdot L^c = A \cdot V_{wind}^b \tag{7}$$

where a, b, c, A are constants depending on wind conditions, L is the collector characteristic length (m). Without going into details about turbulent flows near the corrugation and pores, the surface wind loss from experimental data is fitted into Equation 7. For example, h_{wind} for the normal UTC is evaluated by the following experimental correlation:

$$h_{wind} = 13.041 \cdot V_{wind}^{0.7123} \tag{8}$$

The radiative heat transfer coefficients h_{R1}, h_{R2} and h_{RO} can be obtained from a generic expression for radiation heat transfers between any surface a to surface b:

$$h_{\substack{R \\ a-b}} = \frac{\sigma \cdot (T_a^4 - T_b^4)}{(1/e_a + 1/e_b - 1) \cdot (T_a - T_b)} \tag{9}$$

where σ is the Stephan-Bolzmann constant ($W/m^2/K^4$), T_a and T_b are temperatures (K) at surface a and b, e_a and e_b are emissivity of surface a and b.

For the improved UTC, T_{mid} is the temperature at the transpired absorber, given by:

$$T_{mid} = \frac{Q_{S2} + (h_{R1} + h_{C1}) \cdot T_{surf} + (h_{R2} + h_{C2}) \cdot T_b + MFR \cdot c_p \cdot \varepsilon_{hx} \cdot T_{amb}}{h_{R1} + h_{C1} + h_{R2} + h_{C2} + MFR \cdot c_p \cdot \varepsilon_{hx}} \tag{10}$$

Lastly, T_{plm} is the average of temperature at plenum top, i.e. outlet temperature. According to Dymond&Kutscher's model, T_{plm} for a UTC system is calculated using:

$$T_{plm\_UTC} = \varepsilon_{hx}(T_{surf} - T_{amb}) + T_{amb} \tag{11}$$

Assume that the UTC+TG behaves in a way similar to the normal UTC system in terms of heat transfer from absorber to the plenum air. T_{plm} of UTC+TG can be obtained by simply replacing T_{surf} in Equation 10 with T_{mid}, as the real absorber in the UTC+TG is in fact the middle cladding, whereas the absorber in the normal UTC is the front surface.

Based on the results from Dymond&Kutscher (1997), Van Decker et al. (2001) came up with an expression for calculating effectiveness of transpired collectors:

$$\varepsilon_{hx} = 1 - (1 - \varepsilon_f) \cdot (1 - \varepsilon_h) \cdot (1 - \varepsilon_b) \tag{12}$$

Delisle (2008) refined the embedded constants of this expression of effectiveness to match the test data of a commercial UTC named SolarWall. As laboratory testing (Figure 8a) also uses SolarWall as the normal UTC, its effectiveness used in simulation is given as:

$$\varepsilon_{hx} = 1 - \left[1 + \frac{\max(17.7, 0.708\,\mathrm{Re}_{wind}^{0.5})}{\mathrm{Re}_s}\right]^{-1} \cdot \left[\frac{1}{1 + 3.4\,\mathrm{Re}_b^{-1/3}}\right] \cdot \exp\left(-0.0204\frac{P}{D} - \frac{20.62t}{\mathrm{Re}_h D}\right) \tag{13}$$

$$\mathrm{Re}_{wind} = \frac{V_{wind}P}{\nu} \qquad \mathrm{Re}_s = \frac{V_s P}{\nu} \qquad \mathrm{Re}_b = \frac{V_s P}{\nu\rho} \qquad \mathrm{Re}_h = \frac{V_s D}{\nu\rho} \tag{14}$$

where V_{wind} is wind velocity (m/s), P is distance between pores, i.e. pitch (m), D is diameter of pores (m), ν is kinematic viscosity of air (m^2/s), ρ is porosity of the UTC.

Although the generic form of ε_{hx} (Equation 12) holds true, directly using Equation 13 to calculate effectiveness for UTC+TG system (Figure 8c) gives dissimilar results. Therefore, calibrated effectiveness from experimental data are used in simulations for the UTC+TG system. By definition, effectiveness of any UTC can be obtained from equation 15:

$$\varepsilon_{hx} = (T_{plm} - T_{amb}) / (T_{abs} - T_{amb}) \tag{15}$$

Finally, the thermal efficiency of both UTC and UTC+TG systems can be obtained by:

$$\eta = Q_u / I = MFR \cdot c_p \cdot (T_{plm} - T_{amb}) / I \tag{16}$$

where I is the incident solar radiation (W/m^2) on the façade.

6.2 Thermal Model of PV/T System

Figure 10 below illustrates a simplified thermal network model for a basic PV/T system, where a dark-frame PV panel (1.465m by 0.36m) is mounted as cladding over a flat wall surface. Cold ambient air is actively drawn from the bottom of the PV module and removes heat from the module as it rises. Note that as the height of PV module increases, the thermal efficiency of PV/T decreases.

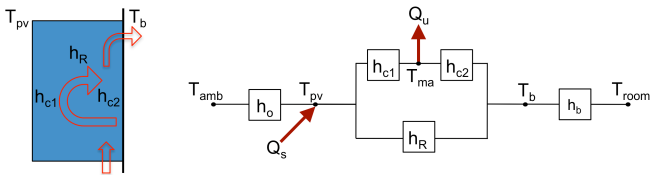

Fig. 10. Simplified Thermal Network Model for PV/T system

The radiative and convective heat transfer coefficients from surface to outside are combined as h_O. Similarly, h_b is the combined coefficient of wall insulation and interior air film. Q_s describes the effective portion of the incident solar radiation converted to heat:

$$Q_s = \alpha_{PV}(1-\eta_{PV})\cdot I \tag{17}$$

where α_{pv} is the overall absorptance of the PV panel (frame and backing included), and η_{pv} is the electric efficiency of the PV panel (typically 10 to 20% for crystalline PV).

Equations containing T_{pv}, T_{ma} and T_b can be listed via the thermal network model. T_{top} is the temperature at the plenum top, while T_{air} is simply the average of T_{top} and T_{amb} (K). For example, T_{pv} and T_{top} can be written as:

$$T_{pv} = \frac{Q_s + h_O T_{amb} + h_R T_b + h_{C1} T_{ma}}{h_O + h_R + h_{C1}} \tag{18}$$

$$T_{top} = \frac{h_{C1}(T_{pv} - T_{air}) + h_{C2}(T_b - T_{air})}{MFR \cdot c_p} + T_{amb} \tag{19}$$

Plenum convective heat transfer coefficients h_{C1} and h_{C2} are calculated from Reynolds number and Nusselt number using equations found in Liao et al. (2007). h_{C1} and h_{C2} vary across the module height (Nusselts number depends on height) and average values are used.

The useful heat collected (Q_u) is given as:

$$Q_u = FR \cdot [Q_s - U_{tot}(T_{air} - T_{amb})] \tag{20}$$

$$FR = \frac{MFR \cdot c_p}{U_{tot}}\left[1 - \exp\left(\frac{-U_{tot} \cdot F}{MFR \cdot c_p}\right)\right], \qquad F = \left[1 + \frac{U_{tot}}{h_{C1} + (h_{C2}^{-1} + h_R^{-1})^{-1}}\right]^{-1} \tag{21}$$

where FR is the heat removal rate assuming an exponential increase of heat removal as MFR increases, U_{tot} is overall loss from the collector to outside and to the back, i.e. h_O and h_b (W/m^2/K). The finite difference method is needed to solve for those variables including Q_u, FR, F and all the temperatures. Calculation details can be found in Chen et al. (2010).

The thermal Efficiency of a simple PV/T system is defined as the fraction of Q_u over incident radiation (I). However, as PV module produces electricity at the same time, a combined thermal equivalent efficiency for PV/T is defined by Athienitis et al. (2011) as:

$$\eta_{PVT\_ThermEquiv} = Q_u / I + COP \cdot [\eta_{PV} \cdot [1 - \beta_{PV}(T_{PV} - T_{STC})]] \tag{22}$$

where COP =4 (coefficient of performance of a heat pump using the generated electricity to produce heat), β_{PV} =0.0046 (PV module temperature coefficient), T_{STC} =25 °C (PV cell temperature at Standard Test Conditions), η_{STC} is the PV electric efficiency at STC.

7 Results and Discussion

7.1 Steady-State Simulation Results compared with Experimental Data

Steady-state simulation and experimental results comparing UTC (Figure 6a, 7a, 8a) and UTC+TG (Figure 6d, 7f, 8c) systems are summarized in Figures 11 and 12. Four exponential curves of efficiency versus flow rate are fitted to experimental data of UTC+TG and UTC systems for visual guidance (Figure 11). Under low wind conditions (V_{wind}=1m/s, blue curves), the efficiency of UTC+TG is 13% to 18% higher than UTC system. As UTC+TG system is less affected by surface wind loss, its efficiency is 23% to 28% higher than that of the conventional UTC system at high wind (V_{wind}=3.5m/s, black curves).

As the effectiveness are calibrated by experimental data (Equation 15) for the UTC+TG model, modelled values were within 4% of experimental measurements at low wind (LW), and within 2% at high wind (HW). In the UTC model, empirical approximation of effectiveness (Equation 13) is employed, resulting in 5.8% maximum difference at HW and 4.5% at LW.

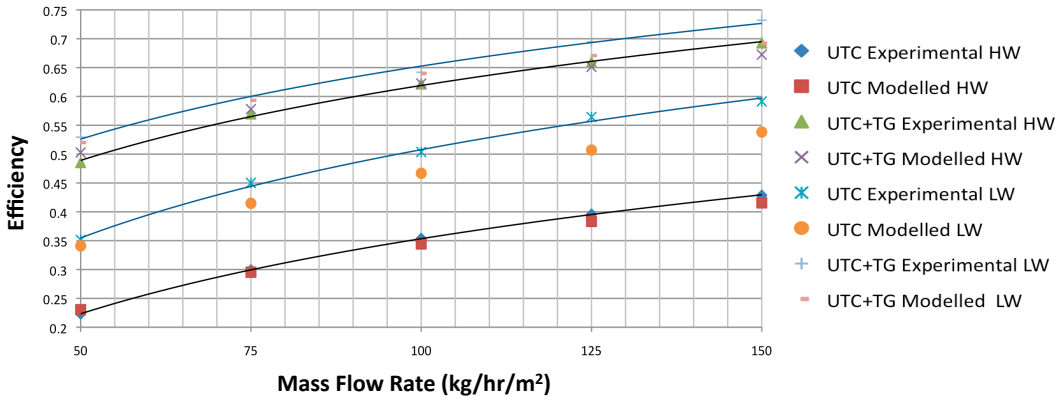

Fig. 11. Steady-state efficiency at different flow rates for UTC+TG and UTC systems

The thermal network models (Section 6.1) also enabled comparison of collector node temperatures. Temperature rise of T_{mid} (absorber) of UTC+TG and T_{surf} (exterior surface) of both UTC and UTC+TG systems are plotted against flow rate in Figure 12. Under both wind conditions, the absorber temperature of UTC+TG (T_{mid}) is higher than the absorber temperature of UTC system (T_{surf}). While T_{mid} remains almost invariant at HW or LW, T_{surf} of UTC is significantly lowered by high wind conditions. As absorber temperature is directly linked to plenum outlet temperature and useful heat delivered, Figure 12 explains the higher efficiency of UTC+TG system due to the reduction of surface convective loss due to wind. As can also be seen from Figure 12, the surface temperature of UTC+TG system is effectively lower than T_{surf} of UTC system, resulting in less surface radiant loss less compared to conventional UTC systems.

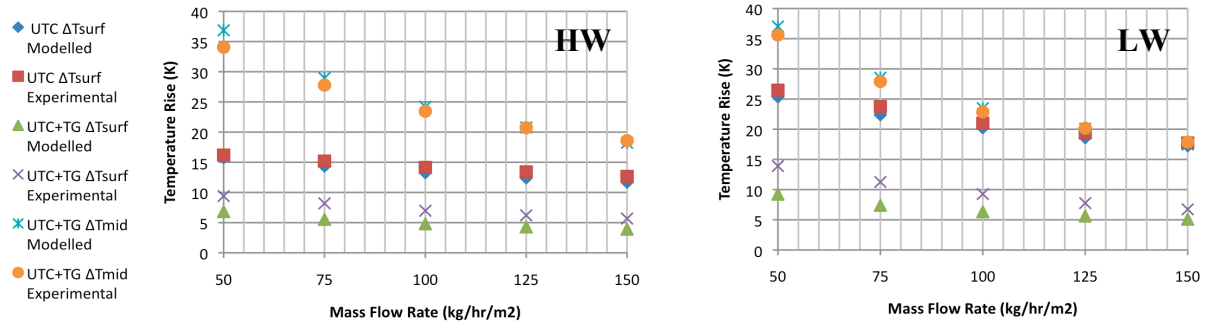

Fig. 12. Surface and Absorber temperature rise at Low Gain condition (838 W/m^2).

The experimental data of UTC+PV/T (Figure 7g, 8d) are compared with simulation results from the simple PV/T model (Section 6.2) in Figure 13 below. Since the simple PV/T model does not consider the corrugated UTC backing on which the PV modules are mounted, the simulation results gives a reasonable absolute difference up to 7% at high flow rates.

To approximate the efficiency of UTC+PV/T+TG (PV coverage 50%, Figure 7h, 8e), the area-weighed sum combining experimental data of UTC+TG (Figure 7f) and simulation results of PV/T model is used. Interestingly, between experimental data of UTC+PV/T+TG and area-weighed sum of UTC+TG and PV/T system, the absolute difference is within 3%.

As shown in Figure 13, by covering the exposed UTC area with transpired glazing (TG 50% coverage), UTC+PV/T+TG system performs 16%-20% higher in efficiency than UTC+PV/T system at high wind and 10%-14% at low wind.

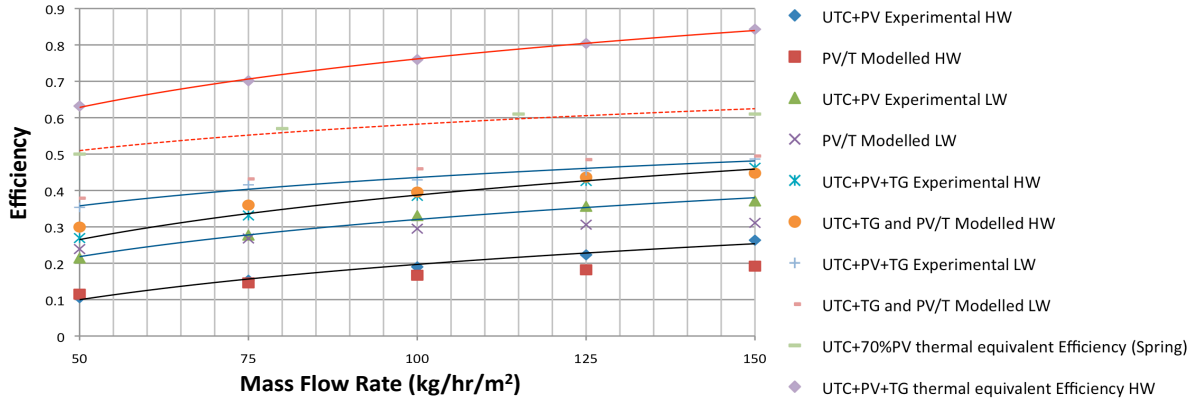

Fig. 13. Efficiency at different flow rates for UTC, CTG, and PV/T systems

Using measured data of the large-scale UTC+PV/T façade of 70% PV coverage seen in Figure 5 (Athienitis et al. 2011) and experimental data of the small UTC+PV/T50%+TG prototype, the combined thermal equivalent efficiency is calculated from Equation 22 and plotted in Figure 13. The thermal equivalent efficiency of UTC+50%PV/T+TG prototype (Figure 13, red curve) is significantly higher than the equivalent efficiency of UTC+70%PV/T façade (red dash curve) , especially at high flow rates.

7.2 Transient Annual Analyses based on Steady State Simulations

Though collector efficiency generally decreases with descending mass flow rate (MFR), plenum outlet temperature actually increases with decreasing MFR. Depending on the end use for the heated air, outlet temperature is useful only within a certain range, whereas too low or too high a plenum temperature does not contribute to the overall energy generation.

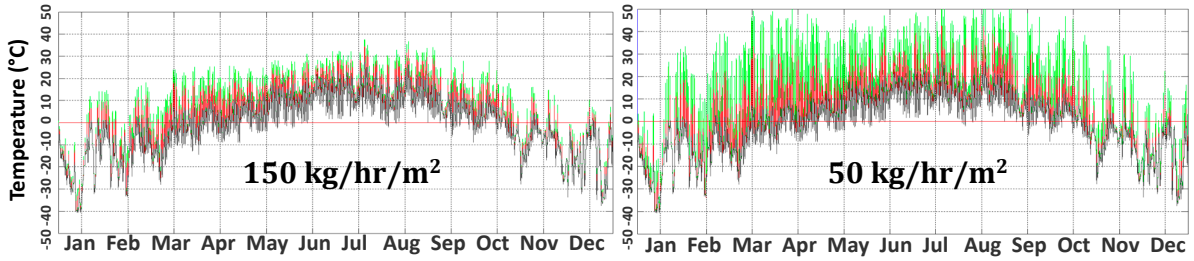

Fig. 14. Plenum temperatures of UTC+TG (green), UTC (red) and T_{amb} (black)

Using the annual weather data of Whitehorse, figure 14 plots the outlet temperature of UTC+TG (green), UTC (red) and outdoor temperature (black) for MFR of 50 and 150 kg/hr/m^2. A wide range of possible plenum temperatures is present depending on the MFR, collector type and weather conditions, which offers crucial flexibility in solar collector design.

Annual analyses using the hourly weather files of three Canadian Nordic cities (Iqaluit, Whitehorse, and Fort Smith) are performed in MATLAB. Results of the three collectors (UTC, UTC+TG, and UTC+PV/T+TG) are summarized in Table 2 below.

Table 2: Annual Simulation results for three Northern locations

Weather Data and Simulation Results		**Iqaluit** NU (63.8°N)	**Whitehorse** YT (60.7°N)	**Fort Smith** NWT (60°N)
Annual average temperature (Coldest Monthly temperature)		-9.4°C (-26.8°C)	-0.9°C (-18.7°C)	-2.9°C (-25.4°C)
Annual average wind speed		4.4m/s	3.8m/s	3.2m/s
Total Heating-Degree days		10,017°C-day	6,915°C-day	7,916°C-day
Annual total Insolation on Façade		4.45 MJ/m^2	4.13 MJ/m^2	4.77 MJ/m^2
Heat Collected by UTC (e.g. SolarWall)	@150kg/hr/m^2	1.9 MJ/m^2	1.86 MJ/m^2	2.2 MJ/m^2
	@50kg/hr/m^2	1.07 MJ/m^2	1.08 MJ/m^2	1.3 MJ/m^2
Heat Collected by UTC+TG	@150kg/hr/m^2	3.15 MJ/m^2	2.92 MJ/m^2	3.38 MJ/m^2
	@50kg/hr/m^2	2.46 MJ/m^2	2.27 MJ/m^2	2.63 MJ/m^2
Heat Collected by UTC+ PV(50%) +TG	@150kg/hr/m^2	1.95 MJ/m^2	1.86 MJ/m^2	2.16 MJ/m^2
	@50kg/hr/m^2	0.931 MJ/m^2	1.01 MJ/m^2	1.22 MJ/m^2
Annual PV potential (solar electricity)		955 kWh/kW	773 kWh/kW	940kWh/kW

Note that not all the solar heat generated by the collectors can be used. The useful fraction of thermal energy depends on end uses and outlet temperature of the solar heated air (e.g. <0°C used to offset HRV defrost coil load, <25°C to offset heating coil load or directly supplied to room, >25°C sent through heat exchanger to heat domestic hot water or sent to storage). Once the desired end uses are determined, collector types and sizes with MFR control strategy can be optimized to regulate outlet temperature and maximizes useful heat.

8 Conclusion

This paper presents the methods and algorithms used for modelling passive and active solar technologies suitable for high-latitude applications. Passive measures of solar utilization can be taken at minimal cost by optimizing interlinked design variables such as house insulation value, south-facing window area and thermal mass. To attain better energy efficiency or even net-zero energy buildings in Nordic climate, façade-integrated solar collectors are suitable for high-performance building envelope such as the SIP system.

Modelling results of several novel façade integrated solar collectors are compared to and calibrated by experimental data obtained from a BIPV/T-SIP prototype. It is found that the performance of conventional UTC as well as UTC+PV/T can be effectively improved (efficiency rise of 10% to 28% in absolute difference) simply by covering with exterior transpired glazing. It is concluded that for cold, windy weather in Northern locations, simple low-cost adaptations like adding transpired glazing creates more resilient and better-suited façade collectors compared to conventional designs.

The findings entail vast design flexibility based on an array of solar collectors that are potentially suitable for high-latitude applications. By combining passive measures of conservation and active generation of on-site solar electric/thermal energy, the building sector in Northern Canada can readily achieve considerable displacement of expensive fossil fuel and its associated transportation cost.

9 Acknowledgements

The project is funded by the Natural Sciences and Engineering Research Council of Canada (NSERC) through the Smart Net-zero Energy Buildings Strategic Research Network and through the Discovery grants of the 2rd and 3rd authors.

10 References

Athienitis, A. K., J. Bambara, B. O'Neill, and J. Faille. 2011. A prototype photovoltaic/ thermal system integrated with transpired collector. Solar Energy

Athienitis, A. K., & Santamouris, M. 2002. *Thermal analysis and design of passive solar buildings*. London: James & James.

Ayoub, J., Dignard-Bailey, L., & Poissant, Y. 2009. *National Survey Report of PV Power Applications in Canada.* International Energy Agency.

Chen, Y., Athienitis, A. K., & Galal, K. 2010. Modeling, design and thermal performance of a BIPV/T system thermally coupled with a ventilated concrete slab in a low energy solar house: Part 1, BIPV/T system and house energy concept. Solar Energy

Delisle, V. 2008. *Analytical and Experimental Study of a PV/Thermal Transpired Solar Collector.* Thesis, University of Waterloo, Waterloo, Ontario.

Dymond, C., & Kutscher, C. 1997. Development of a flow distribution and design model for transpired solar collectors. Solar Energy

Leon, M. A., & Kumar, S. 2006. Mathematical modeling and thermal performance analysis of unglazed transpired solar collectors. Solar Energy

Liao, L., Athienitis, A. K., Candanedo, L., Park, K.-W., Poissant, Y., & Collins, M. 2007. Numerical and Experimental Study of Heat Transfer in a BIPV-Thermal System.

National Energy Board. 2011. Energy Use in Canada's North.

Natural Resources Canada. 2007. Photovoltaic potential and solar resource map of Canada

Norling, C. R.; Rode, C.; Svendsen, S.; Kragh, J.; Reimann, G., 2006. A low-energy building under arctic conditions, In 3rd International Building Physics Conference, Montreal

Palyvos, J. A. 2008. A survey of wind convection coefficient correlations for building envelope energy systems' modeling. Applied Thermal Engineering

Poissant, Y. 2009. Field assessment of novel PV module technologies in Canada. Natural Resources Canada. Varennes.

Poissant, Y., Thevenard, D., & Turcotte, D. 2004. Performance monitoring of the Nunavut Arctic College PV system: Nine years of reliable electricity generation.

TamizhMani, G.; Dignard-Bailey, L.; Thevenard, D.; Howell, D. G., 1998. Influence of low-light module performance on the energy production of Canadian grid-connected PV systems. In Renewable Energy Technologies in Cold Climates, Montreal

Van Decker G. W. E., Hollands K. G. T., and Brunger A. P. 2001. Heat-exchange relations for unglazed transpired solar collectors with circular holes on a square or triangular pitch. Solar Energy

Vladykova, P.; Rode, C.; Nielsen, T. R.; Pedersen, S. 2008. *Passive Houses for Arctic Climates*, In 1st Nordic passive house conference, Trondheim, Norway.

Yukon Housing Corporation. 2009. SuperGreen Energy Efficiency.